$\Gamma_1) > 20$ mN m^{-1}. Under these conditions the predicted composition of the mixed VBLS + EL monolayer $x_2 = 0.2$ corresponds to 1/4 VBLS/EL (mol/mol), and the molar free energy of EL molecules is 1.7 kcal/mol superior to that in the pure monolayer. These conclusions are qualitatively opposite to the classical ones based on the commonly accepted belief that when $\Delta\Pi = 0$, no penetration has taken place and $\Gamma_{2,0} = 0$.

Registry No. VBLS, 143-67-9.

Applications and Limitations of Boundary-Line Fractal Analysis of Irregular Surfaces: Proteins, Aggregates, and Porous Materials

Dina Farin,† Shmuel Peleg,‡ David Yavin,‡ and David Avnir*†

Departments of Organic Chemistry and Computer Sciences, The Hebrew University of Jerusalem, Jerusalem 91904, Israel

Received December 7, 1984

Computerized image analysis techniques are developed for fractal analysis of boundary lines of objects possessing irregular surfaces. The objects analyzed are proteins, a catalyst, macroporous silica gel, simulated colloidal flocs, and a carbon black aggregate. Application to stylus profilometry is demonstrated. It is shown that the standard fractal line analyses are insensitive and may lead to questionable interpretations. More sensitive methods are presented and used to reanalyze previous reports and to investigate the applicability of the concept of self-similarity in nonstatistical analyses. Conditions under which line fractal dimension is indicative of surface roughness are briefly discussed.

1. Introduction

Chemical processes at interfaces are governed by three main parameters: (a) the chemical and physical properties of the functional groups at the surface (these functional groups may vary from a plethora of species such as found at the surfaces of carbon blacks to the relatively simple chemistry found at the surfaces of many metal oxides), (b) the distribution of active (not necessarily catalytic) sites at the surface (here one can mention the on-going debate regarding clustering of silanols at the surface of silica),[1] (c) the geometry of the surface. The first parameter, and to a certain extent the second one, has been studied so far by tools that have long been developed for homogeneous solutions. The extrapolation from solutions to surfaces was possible in this case, since the chemistry of, say, an OH group is basically the same whether this group is part of a solvent molecule or a surface moiety. This straightforward extrapolation is not possible, however, for the third parameter, surface geometry: in solution, a solute molecule is surrounded by a spherical symmetric solvent shell and its translational movements are governed by Brownian collisions, by concentration gradients, and by convections. In contradistinction to solution, surface cage properties and surface translation are strongly dependent on geometry. "Solvation" on a surface is nonisotropic, the fixed-geometry cage has no dynamical character of formation, and diffusion is governed by the wiggles of the surface. Investigation of the geometrical problem is further complicated by the fact that unless special precautions and procedures are taken,[2] material surfaces do not possess a simple flat two-dimensional geometry. In contrast, the majority of surfaces are fractured, stepped, convoluted, and very irregular. The need for a practical, simple yet powerful tool for characterization of surface irregularity is emphasized by the impressive list of surface phenomena that are strongly dependent on this geometric factor: adsorption/desorption hysteresis loops, catalysis, conformation of adsorbates, diffusion on surfaces, crystal growth, drug dissolution, spectral properties of adsorbates (e.g., enhanced Raman spectrum), scattering of irradiation and projectiles, and chromatography—to mention just a few.

The classical treatment of surface irregularity has been to regard it as a deviation from an ideal reference, e.g., a plane,[3] or to regard it as superposition of regular periodic functions (Fourier transforms[4]). Mandelbrot has suggested recently a different approach to natural irregularity in general, an approach that has an inherent appeal—it does not treat the irregularity as a pathological deviation but takes it as a starting point.[5] By this approach the degree of irregularity is given by the fractal dimension, $1 \leq D < 2$ for lines and $2 \leq D < 3$ for surfaces, so that the higher D is, the more wiggly the object is. D is obtained from a resolution analysis: the rate of appearance of new features of the irregularity as a function of the size of the probing yardstick (or degree of magnification) is measured. An object is a fractal if this rate is given by the power law

$$n \propto r^{-D} \tag{1}$$

where n is the number of yardsticks of size r needed to measure the total length of the wiggly line. For a smooth curve, eq 1 becomes the familiar $n \propto r^{-1}$; for a wiggly line, see Figure 1 for visualization of the equation. Equation 1 has been widely interpreted as reflecting scaling self-similarity (ref 5 and most of the fractal analyses cited

† Department of Organic Chemistry.
‡ Department of Computer Science.

(1) (a) Unger, K. K.; Roumeliotis, P. J. *J. Chromatogr.* **1978**, *149*, 211. (b) Unger, K. K. "Porous Silica"; Elsevier: New York, 1979. (c) Lochmuller, C. H.; Colborn, A. S.; Hunnicutt, M. L. *Anal. Chem.* **1983**, *55*, 1344.
(2) Somorjai, G. A. "Chemistry in Two Dimensions: Surfaces"; Cornell University Press: Ithaca, NY, 1981.
(3) Thomas, T. R. "Rough Surfaces"; Longman: London, 1982.
(4) Beddow, J. K., Meloy, T. P., Eds.; "Advanced Particulate Morphology"; CRC Press: Boca Raton, FL, 1977.
(5) Mandelbrot, B. B. "The Fractal Geometry of Nature"; Freeman: San Francisco, 1982.

0743-7463/85/2401-0399$01.50/0

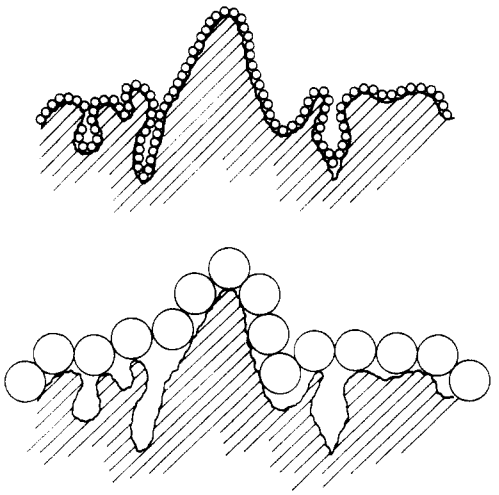

Figure 1. Visualization of eq 1. For a wiggly surface boundary, the total length grows faster than $n \propto r^{-1}$ (n, the number of discs; r, disc radius).

below). The generality of this interpretation is questioned in this article with respect to nonstatistical analyses.

In a recent series of papers,[6] Pfeifer and we have developed the use of adsorption data for the determination of fractal properties of surfaces at the molecular-size range. Our main discovery has been that the surfaces of most materials, amorphous and crystalline, porous and nonporous, synthetic and natural, are fractals.[6e] The key idea in that investigation was to use molecules as yardsticks of varying sizes by methods derived from eq 1. By definition then, information that is obtained by these methods on geometric irregularity covers the molecular scales. For reaction–diffusion studies on fractal surfaces, it becomes important, however, to determine the fractal dimension at larger scales, e.g., at distances that a reactant or an excited state diffuses before reacting. Such larger scales of roughness are also important for a variety of applications such as adhesion, particle rheology, corrosion, and optical performance. Whereas good resolution of molecular-size features is still beyond the power of most of the contemporal imaging techniques,[7] diffusional distances, say of 50 Å and up, do enter the domain of these techniques. Consequently we have launched recently[8] a project aimed at elucidating the fractal dimension of surfaces by analyses of (electron) microscope pictures. Magnifications need not, of course, be only optical; stylus traces[3] and molecular models are two other possibilities analyzed below. So far we have inferred supramolecular ranges (up to 100 Å) only indirectly by assuming particle similarity at least down to the finest resolution (smallest adsorbate).[6c,e,h] Image analysis techniques have the potential to test directly this assumption through partial overlap of the probing ranges of the two independent experimental methods. The limitations of Fourier analysis of irregular lines have been discussed elsewhere.[6f]

Determination of scaling properties of surface features by image analysis requires, in principle, stereoscopic techniques. While these three-dimensional analysis tools are still at the developmental stage, useful information is already available from reduced dimensionality techniques. Fractal resolution analysis of two-dimensional objects (e.g., a picture of a three-dimensional object, a texture) are now possible; the technique has recently been developed[8] and its application to electron microscope textures will be given elsewhere. It is remarkable that useful information on the fractal nature of surfaces may be obtained even by cautious (see below) analysis of lines. In fact the idea of using a trace line, such that is obtained by stilus profilometry, as a representative of *surface* geometry is one of the cornerstones in the study of surface roughness.[3]

The implementation of fractal analysis of boundary lines is spreading fast in many domains of natural sciences. Examples are the fractal analyses of the boundaries of rain clouds,[9] of mitochondria membranes,[10] and of diffusing liquid fingers.[11] Three principal methods are used: length measurement as a function of resolution (i.e., yardstick size and other dilation processes),[5] perimeter/area analysis at fixed resolution,[5] and length measurement as a function of optical magnifications, measured with a fixed yardstick.[10,12] Of special interest for the study reported here are the line analyses of materials. These include fractures surfaces of metals,[13,14] quartz particles,[15] and a wide variety of other particulate materials, as described by Kaye.[16] A number of authors[16-18] found interest in a picture of a colloidal carbon floc published by Medalia[19] (Figure 6a) and described it as a fractal object. It is the ease of the technique and its widespread use that prompt us to reinvestigate this analytical tool with special emphasis on nonstatistical interpretations. We describe a computerized method for the line analyses; we use sensitive straight line tests and come to the following conclusions: (a) A boundary line that obeys eq 1 need not be self-similar. (b) Nonstatistical strict self-similarity is scarce. (c) Even in the absence of self-similarity, the exponent D in eq 1 carries useful information in the original spirit of Richardson coast-line analyses,[5,20] i.e., an empirical relation between scales and measured object. However, (d) eq 1 is quite insensitive for detailed analysis of local, short-range resolution variations. It must be replaced by more sensitive methods, two of which are described below. (e) Equation 1 with $D < 1.2$ describes well virtually all low-irregularity lines tested by us and others, even lines that are clearly not self-similar.

2. Length Measurements by Computerized Image Analysis Techniques

2.1. The Method. Boundary lines were reproduced

(6) (a) Avnir, D.; Pfeifer, P. *Nouv. J. Chim.* **1983**, *7*, 71. (b) Pfeifer, P.; Avnir, D.; Farin, D. *Surf. Sci.* **1983**, *126*, 569. (c) Pfeifer, P.; Avnir, D. *J. Chem. Phys.* **1983**, *79*, 3558. (d) Avnir, D.; Farin, D.; Pfeifer, P. *J. Chem. Phys.* **1983**, *79*, 3566. (e) Avnir, D.; Farin, D.; Pfeifer, P. *Nature (London)* **1984**, *308*, 261. (f) Pfeifer, P. *Appl. Surf. Sci.* **1984**, *18*, 146. (g) Pfeifer, P.; Avnir, D.; Farin, D. *J. Stat. Phys.* **1984**, *36*, 699. (h) Avnir, D.; Farin, D.; Pfeifer, P. *J. Colloid Interface Sci.* **1985**, *103*, 112. (i) Farin, D.; Volpert, A.; Avnir, D. *J. Am. Chem. Soc.* **1985**, *107*, 3368–3370.

(7) For a recent exception, see, e.g.: Hovmuller S.; et al. *Nature (London)* **1984**, *311*, 238.

(8) Peleg, S.; Naor, J.; Hartley, R.; Avnir, D. *IEEE Trans. Pattern Anal. Mach. Intelligence* **1984**, *6*, 518.

(9) Lovejoy, S. *Science (Washington, D.C.)* **1982**, *216*, 185.

(10) Paumgartner, D.; Losa, G.; Weibel, E. R. *J. Microsc. (Oxford)* **1981**, *121*, 51.

(11) Nittmann, J.; Daccord, G.; Stanley, E. *Nature (London)* **1985**, *314*, 141.

(12) Serra, J. "Image Analysis and Mathematical Morphology"; Academic Press: New York/London, **1982**; pp 127–161.

(13) Mandelbrot, B. B.; Passoja, D. E.; Paullay, A. J. *Nature (London)* **1984**, *308*, 721.

(14) (a) Chermant, J. L.; Coster, M. *J. Mater. Sci.* **1979**, *14*, 509. (b) Coster, M.; Chermant, J. L. *Int. Met. Rev.* **1983**, *28*, 234.

(15) Orford, J. D.; Whalley, N. B. *Sedimentology* **1983**, *30*, 655.

(16) (a) Kaye, B. H. "Direct characterization of Fine Particles"; Wiley: New York, 1981; pp 367–378. (b) Kaye, B. H. In "Modern Methods of Fine Particle Characterization"; Beddow, J. K., Ed.; CRC Press: Boca Raton, FL, in press. (c) Kaye, B. H. Research Report 21, Institute for Fine Particle Research, Laurentian Univ., Sudbury, Ontario, Canada, 1978.

(17) Flook, A. G. *Powder Technol.* **1978**, *21*, 295.

(18) Schwarz, H.; Exner, H. E. *Powder Technol.* **1980**, *27*, 207.

(19) Medalia, A. I. In "Surface and Colloid Science"; Matijevic, E., Ed.; Wiley: New York, 1971; Vol. 4, pp 1–92.

(20) Richardson, L. F. *Gen. Syst. Yearb.* **1961**, *6*, 139.

from pictures of the objects. If the object is of one shade only and the background of another, boundary line reproduction is unnecessary. The boundary to be analyzed was videophotographed with a camera and digitized on a 512 × 512 pixel grid using a Grinell image processing system linked to a general purpose computer (Vax, Digital). Boundary regions were extracted from the Digital images and then represented by a sequence of numbers in the range 0–7. Each number represents the relative location to the previous point, using the following scheme, relative to P:

3	2	1
4	*P*	0
5	6	7

Thus, the line represented by 0–6–0–2–2–0–6–0–2–0–6 is

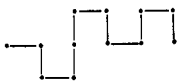

Further details of this procedure may be found in ref 21.

For length measurements, we assume the line is straight between any two consecutive points. Given a yardstick length r (r can be any real value), we choose a starting point and walk the yardstick along the line. We do the walking by moving continuously along the line, until we reach the first point P on the line with "aerial" distance r from the starting point. We count this as the first step of the yardstick and continue again from the point P. Neither the starting point nor the point P should be grid points. Since in most cases one cannot cover the entire line with an integral number of yardsticks, the termination should be handled differently. Out of several possible approaches we chose to take the straight line segment between the current point and the end point of the line. We add the length of this line segment to the total length, and the ratio of its length to the yardstick's length is added to the yardstick count. Other methods are possible (see, for example, ref 18), but there is no definite advantage to any method. With small yardsticks the termination treatment does not make a substantial difference. The fractal dimension is then calculated from eq 1. The smallest yardsticks for which the trivial $D = 1.0$ is obtained were omitted. The largest yardstick used did not exceed 20% of the object's diameter. A 50-pixel reference line is indicated in the figures. In case the boundary line has gaps (e.g., Figure 3a), the total number for all line fractions was taken. For all yardsticks, $r_{i+1}/r_i = 1.2$. Starting the yardstick count at different points or rotating the picture did not affect D values. The line thickness causes slight changes in D whether the outer or the inner pixels are taken. As a standard we took the inner pixels. Hand instability at the boundary line reproduction stage, does not affect D. In order to evaluate how much is lost by the imaging process, two objects of known fractal dimension were analyzed. The first was a limited Koch curve constructed by six iterations.[5] A theoretical Koch curve yields 1.26...; the limited six iteration curve, constructed as a number chain code in the computer memory, resulted in an expected lower value of 1.22 ± 0.01. Analysis of an image of the limited curve gave the same value (Table 3.Cf. ref 17, 18). The second object was the random hexasquig on p 231 in ref 5. Image analysis of the figure on that page resulted in $D = 1.31 \pm 0.01$. The theoretical value is 1.33...[5]

2.2 Comments on Some Other Methods of Fractal Line Analysis. It is beyond the scope of this article to critically review the many variations of methods for determination of line fractality. A few comments, however, will be made.

The idea of walking a yardstick along a line dates back to Richardson[20] and was manually implemented by many authors, e.g., Kaye.[16] Semiautomated analysis was reported by a number of investigators[14,17,18] who used variations of the dilation method:[5] the line is covered by digital circles of radius r, and the total covered area is then divided by $2r$ to give the measured length. The dilation methods fail, however, to measure length of plane-filling lines, as dilation with any circle of positive radius will yield the same area: the entire plane. Kaye, in his manual "swing of a compass" method,[16] takes the first intersection encountered. This, too, will fail when lines are plane filling. It should be mentioned, however, that for cases of shapes and sets of points on the plane, the dilation method[8] yields good results. Others (e.g., ref 15) have measured distances *on* the analyzed line itself. The paradox is, of course, using the object's length to measure its length. Aside from lacking theoretical justification, distances along the curve are inaccurate and resolution dependent.

Finally, it should be mentioned that automated image analysis has been used in the very active field of fractal aggregates.[22] The most common method is analysis of mass distribution. The fractal dimension thus obtained may coincide with the boundary line fractal dimension (the hull dimension[23]), under special conditions.[11,23]

Table I. Fractal Dimensions of Boundary Lines of Some Proteins

protein		fractal dimens[b]
mouse immunoglobulin A Fab McPc 603	front view	1.129 ± 0.006
	bottom view	1.145 ± 0.007
bacterial serine protease A		1.088 ± 0.002
chicken lysozyme		1.118 ± 0.006
subtilisin inhibitor, BPN′ complex dimer		1.110 ± 0.004
α-cobratoxin[a]		1.133 ± 0.007
cytochrome C3		1.117 ± 0.004
ribosomal protein L7/L12	bottom view	1.132 ± 0.006
	front view	1.102 ± 0.007
	right view	1.125 ± 0.008

[a] See Figure 2. [b] All correlation coefficients: 0.9996–0.9999.

3. Standard Fractal Dimension Determination of Selected Irregular Surfaces

By the technique described in section 2, a number of irregular surfaces, all of which have been reported and described previously, were analyzed. In these analyses it is assumed that $D_{surface} = D_{line} + 1$.[5] This assumption, which has been routinely used also in other studies,[10,13] is valid only for isotropic objects and is further discussed in section 4.

Proteins. Two research groups have analyzed the irregular structure of proteins in fractal terms.[24,25] These groups were interested in the fractal dimension of the wiggled polypeptide backbone. Our point of view is different: proteins interact with the environment through the interface. Therefore surface accessibility of the proteins[26] seems to us of greater relevance to the under-

(21) Rosenfeld, A.; Kak, A. "Digital Picture Processing"; Academic Press: New York, 1981.

(22) E.g.: Matsushita, M.; Sano, M.; Hayakawa, Y.; Honjo, H.; Sawada, J. *Phys. Rev. Lett.* **1984**, *53*, 286.

(23) Voss, R. F. *J. Phys. A: Math. Gen.* **1984**, *17*, L373.

(24) Allen, J. P.; Colvin, J. T.; Stinson, D. G.; Flynn, C. P.; Stapleton, H. J. *Biophys. J.* **1982**, *38*, 299.

(25) Yoshinori, I.; Toshyuki, I. *J. Phys. Soc. Jpn.* **1984**, *53*, 2162.

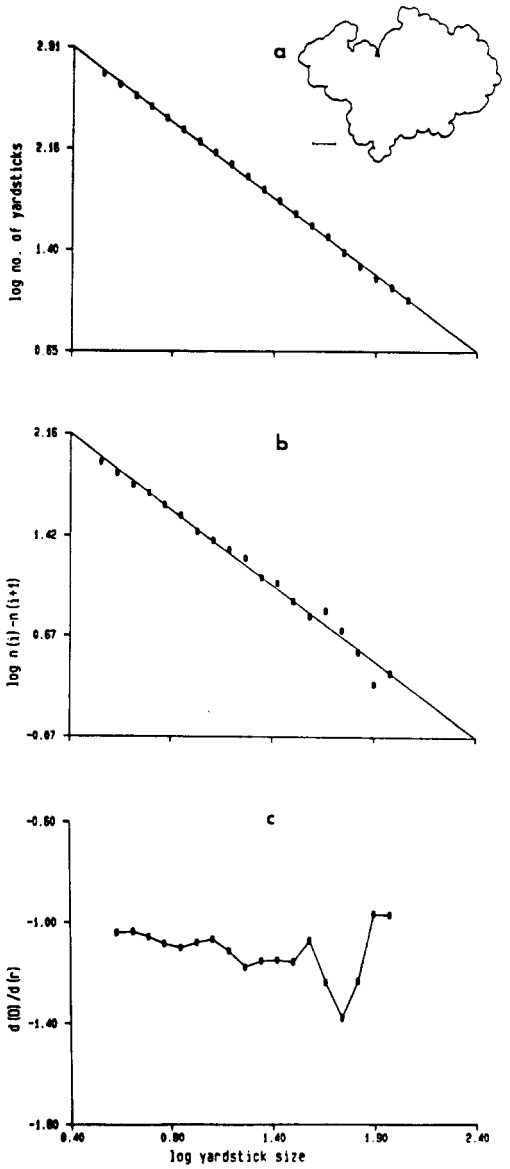

Figure 2. Number of yardsticks (a), the difference in number of yardsticks (b), and local slope (c), as a function of yardstick size (in pixels) for a protein (α-cobratoxin) silhouette.

standing of protein-involved processes (e.g., enzymatic catalysis).[6d]

Seven proteins were analyzed by taking the silhouettes of computerized space-filling models (Figure 2a) as reported by Feldmann.[27] Two of these were analyzed from more than one viewpoint. The results are collected in Table I. Excellent straight lines are obtained (Figure 2a), with D values around 1.1, significantly lower than backbone fractal dimensions.[24,25] The data in Table I is further discussed in section 4. Pfeifer et al. have employed recently section boundary lines of lysozyme in a similar approach.[28]

Pt Black Catalyst. Barna et al. have studied the morphology of Pt black catalysts.[29] Typically for such studies, the report is accompanied by many pictures showing the morphology of various Pt blacks, as the only

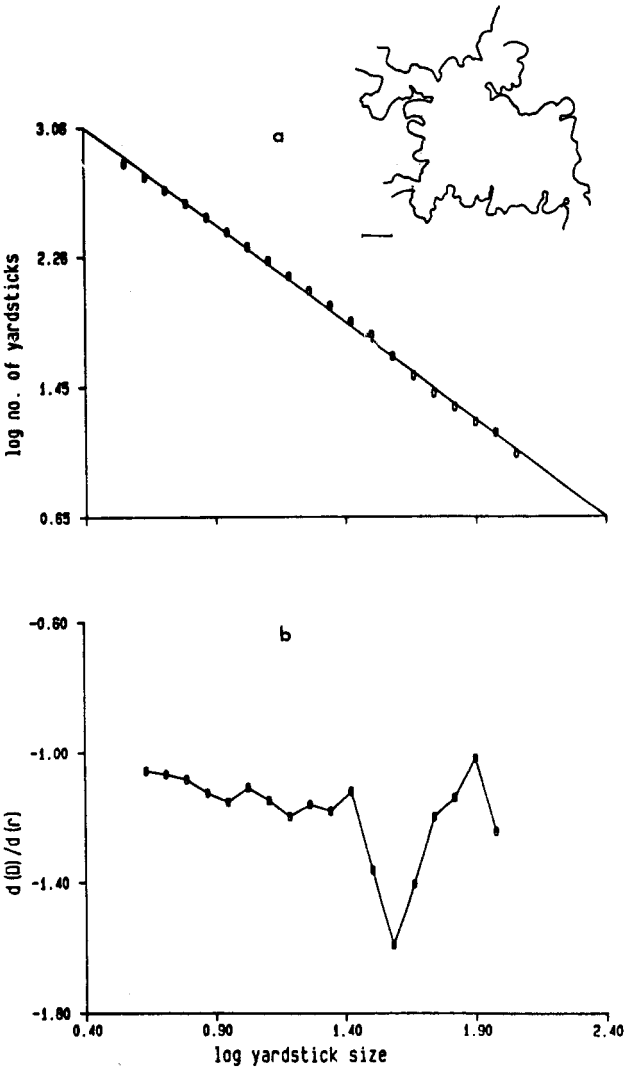

Figure 3. Number of yardsticks (a) and local slope (b), as a function of yardstick size (in pixels) for Pt black catalyst.

means to present the geometrical features of the catalyst. The fractal approach opens the possibility of characterizing the irregularity of catalysts by a single number. This is exemplified on one of Barna's catalysts (Figure 3a in ref 29, Figure 3a in this article) for which $D = 1.20 \pm 0.01$ (correlation coefficient, −0.999) is obtained. For a discussion of fractal catalysts, see ref 6c,g.

Porous Silica Gel. This common adsorbent has been the subject of intensive investigation[6a,g,h,i] from which it was concluded that at the molecular range, the fractal dimension of the surface is close to the limit $D_{surface} \rightarrow 3.0$. Small-angle X-ray scattering results are in agreement.[30] Unger and Gimpel have published a scanning electron micrograph of a novel chromatographic macroporous silica (LiChrosphere Si 4000; average pore diameter 4000 Å).[31] The boundary line of the pore entrances was reproduced and analyzed (Figure 4a), to yield $D = 1.36 \pm 0.03$ (correlation coefficient, −0.997); i.e., $D_{surface} \simeq 2.4$ at a range which is far beyond molecular scales.

Sutherland's Simulated Flocs. As mentioned in section 2, fractal analyses of aggregation processes and of the resulting clusters have gained intensive attention in recent years.[22,23] All reports except the very recent study by Voss[23] were interested in the scaling properties of the mass distribution (e.g., number of particles as a function

(26) Lee, B.; Richards, F. M. *J. Mol. Biol.* **1971**, *55*, 379.
(27) Feldmann, R. *Proceedings of the 7th Annual Katzir-Katchalsky Conference*, Rehovot and Nof-Ginossar, Israel, 1980. (Protein photographs distributed by the author.)
(28) Pfeifer, P.; Welz, V.; Wippermann, H. *Chem. Phys. Lett.* **1985**, *113*, 535.
(29) Barna, A.; Barna, P. B.; Toth, L.; Paal, Z.; Tetenyi, P. *Appl. Surf. Sci.* **1982–1983**, *14*, 85.
(30) Bale, H. D.; Schmidt, P. W. *Phys. Rev. Lett.* **1984**, *53*, 596.
(31) Unger, K. K.; Gimpel, M. G. *J. Chromatogr.* **1979**, *180*, 93.

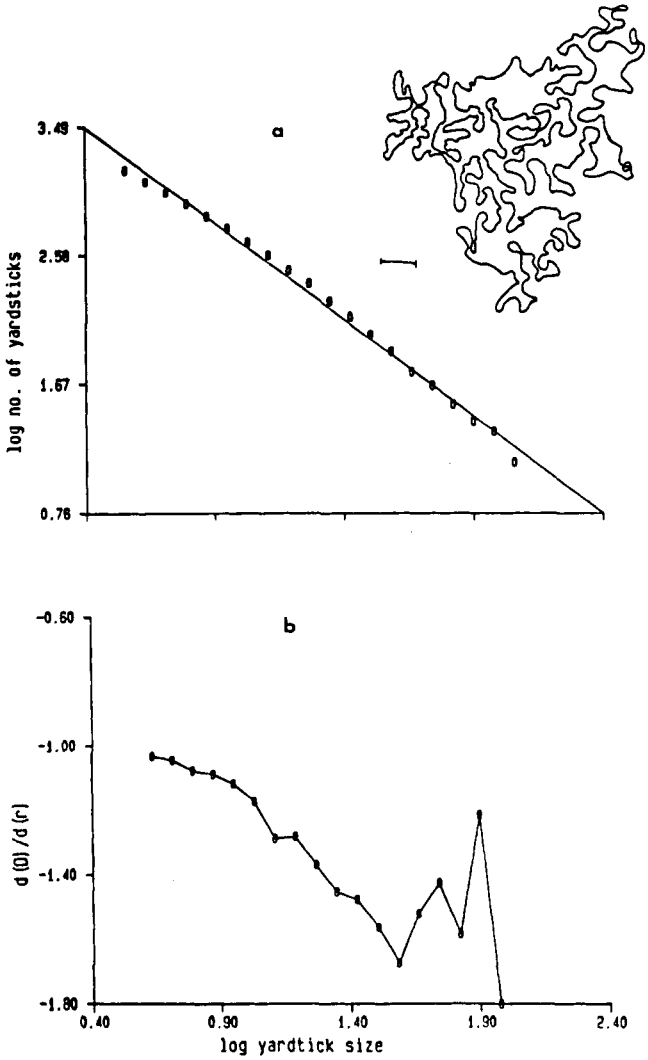

Figure 4. Number of yardsticks (a) and local slope (b), as a function of yardstick size (in pixels), for macroporous silica gel, LiChrosphere Si 4000.

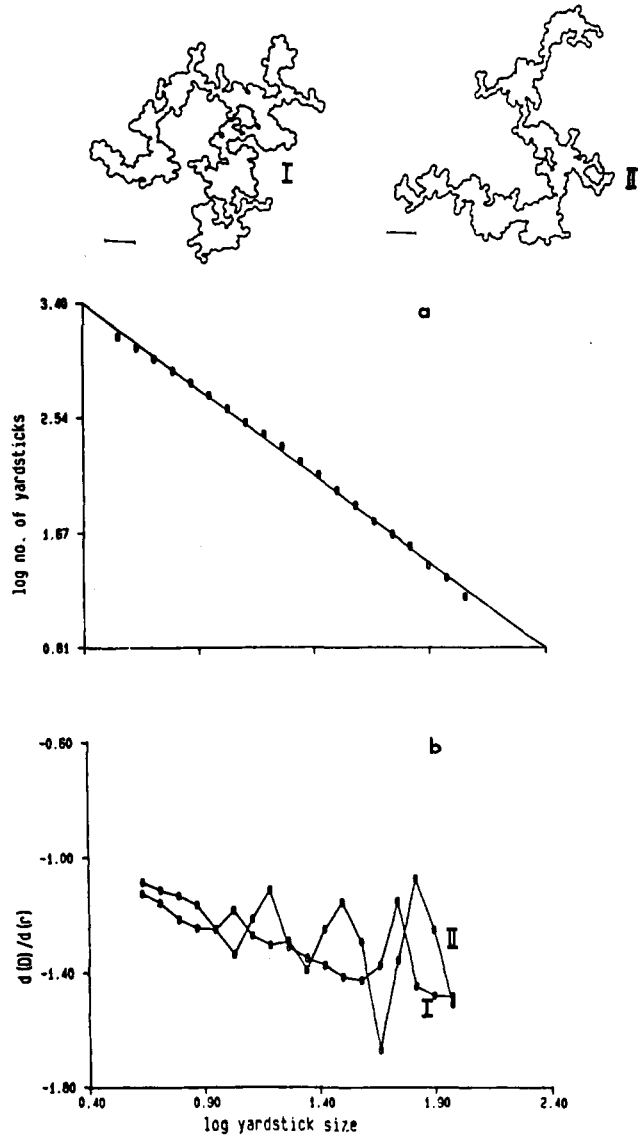

Figure 5. Sutherland's simulated flocs. (a) Number of yardsticks as a function of yardstick size (in pixels) for the left floc. (b) Local slopes as a function of yardstick size (in pixels) for the left (I) and right (II) flocs.

of the distance from the cluster center). Since many high surface area materials, such as silica aerogel, are formed by clustering and condensation of microspheres,[32] it seemed to us that fractal analysis of the *surface* of such clusters (the cluster "hull"[5,23]) is of interest. We chose to analyze the perimeter of simulated flocs, as reported by Sutherland.[33] This study is a pre-fractal-era (1967) cluster–cluster–aggregation model. It is based on Schmoluchowski's model in which an i-fold cluster and a j-fold cluster yield an $(i + j)$-fold cluster until there is only one big floc. Such a model gives a decreasing weight to single-particle addition as the process goes on. Two flocs of 601 particles each (Figures 3 and 4 in ref 33; Figure 5a in this article) were reproduced and analyzed as described in section 2. It is remarkable to find out that eq 1 describes the two flocs very well, and that both yield virtually the same value: $D = 1.29 \pm 0.01$ (left) and $D = 1.28 \pm 0.01$ (right) (correlation coefficient for both, −0.999).

Medalia's Carbon Black Aggregate. Medalia published more than a decade ago a picture of a carbon black aggregate.[19] As mentioned above, the boundary line of this aggregate was analyzed by three groups. All claim that this is a fractal object with a D value of 1.07 and 1.37,[17] 1.13,[18] and 1.19.[16] We find (Figure 6a) $D = 1.10 \pm 0.01$ (correlation coefficient −0.999) but question below the self-similarity interpretation of this single object.

Table II. Effect of Changes in Stylus Radius on Trace Length

length, pixels	stylus radius, μm
2617	2.5
1731	50
790	280
401	1700
389	3200

Stylus Profilometry. The technique is based on the principle of providing a section of the surface by recording the trace of the ups and downs of a diamond stylus probing a surface.[3,34] This convenient technique is in use in a wide variety of applications, as exemplified in our recent work on fluorescent silica thin films prepared by the sol/gel method.[35] It is interesting to notice that this technique provides a direct method for fractal analysis by measuring the length of the trace as a function of styli radii either

(32) Zarzycki, J.; Parssas, M.; Phalippou, J. *J. Mater. Sci.* **1982**, *17*, 3771.
(33) Sutherland, D. N. *J. Colloid Interface Sci.* **1967**, *25*, 373.
(34) Radhakrishnan, V. *Wear* **1970**, *16*, 325.
(35) Avnir, D.; Kaufmann, V. R.; Reisfeld, R. *J. Non-Cryst. Solids*, in press.

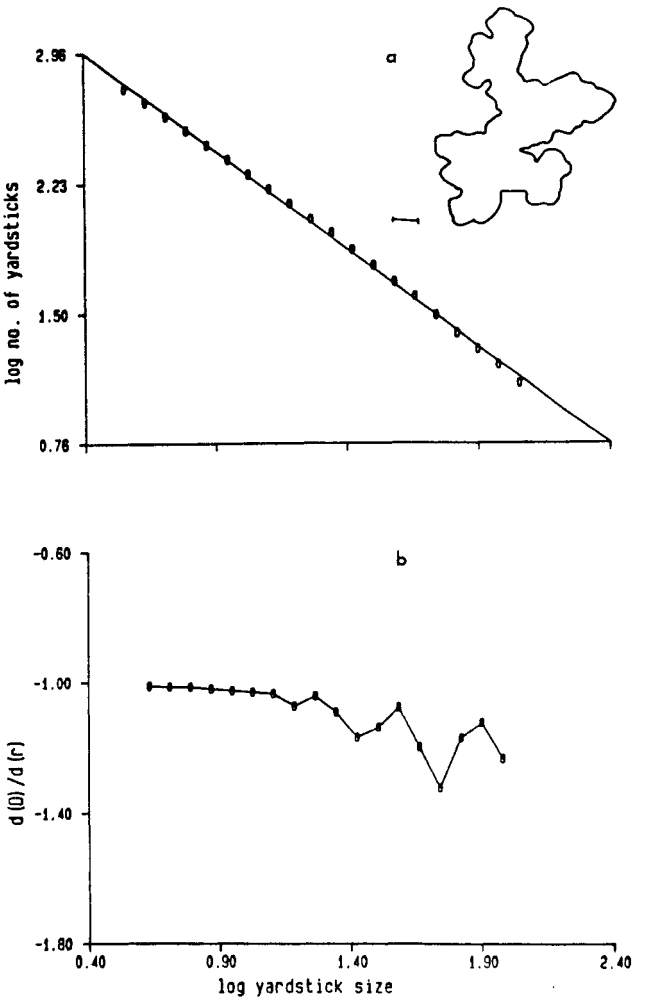

Figure 6. Number of yardsticks (a) and local slope (b) as a function of yardstick size (in pixels) for Medalia's carbon particles floc.

by actually replacing the styli or by computing coarser traces from the finest one.[34] The second possibility is in fact equivalent to the procedure described in section 2. Radhakrishnan measured the surface face of a milled sample with a 2.5-μm stylus and computed the traces obtained from coarser styli.[34] We calculated the fractal dimension by measuring the lengths of the traces from Figure 3 in ref 34 as a function of styli radii (Table II) and compared the results to the analysis of the finest trace by the method described above. Indeed, virtually the same D values were obtained: $D = 1.29 \pm 0.04$ for the first method and $D = 1.25 \pm 0.02$ for the latter. And so, what is called "a source of error" (i.e., variations in styli radii, p 21 in ref 3) carries in fact useful information.

4. Interpretation of the D Values

As we have seen in the previous section, the exponent D provides useful information on the overall degree of irregularity. However, since D values are obtained from log/log plots which have a known smoothing effect, and since the experimental points can occupy only a very limited zone in the log n – log r plane (see, e.g., the zone for $1.0 < D < 1.5$ in Figure 7), there is a danger of insensitivity which may hide useful information and lead to erroneous interpretations.

As an example we look at a regular sawtooth (Figure 8a) which is obviously not fractal and not self-similar. If this object is analyzed by the standard technique, with a reasonable range of yardsticks, as used for all other objects,

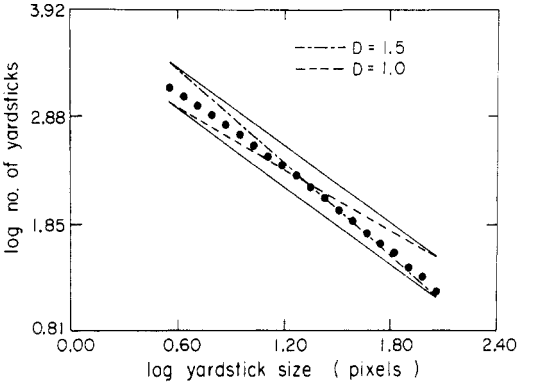

Figure 7. Low sensitivity of log n vs. log r plots of eq 1 demonstrated on the left floc in Figure 5. Cf. also the derivative on Figure 5b.

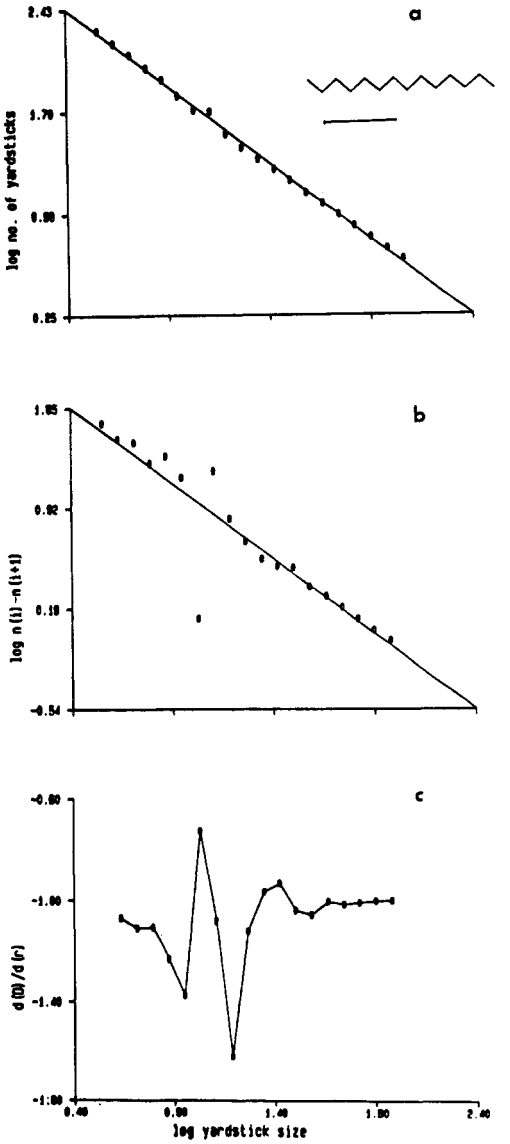

Figure 8. Number of yardsticks (a), the difference in number of yardsticks (b), and local slope (c), as a function of yardstick size (in pixels), for a sawtooth.

a good "fractal dimension" is obtained: $D = 1.09 \pm 0.01$ (correlation coefficient, –0.999). Similarly the early stages of the construction of Koch curve (first iteration, a straight line (the initiator); second iteration, the generator Λ; and so on up to the seventh iteration[5]) yield progressively larger D values (Table III, Figure 9a) approaching the limit 1.26... It is true that by proper choice of yardsticks (exactly

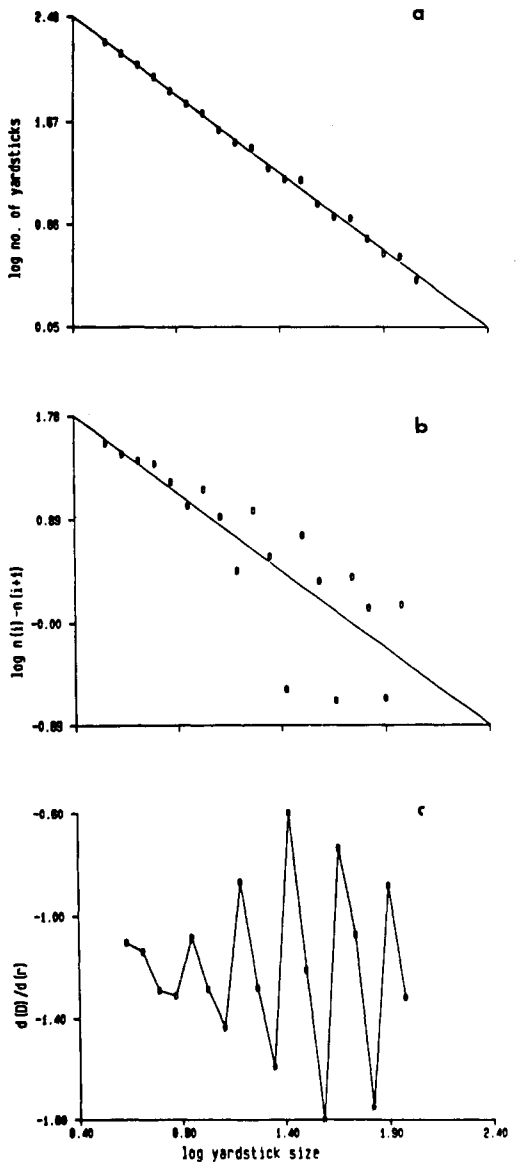

Figure 9. Number of yardsticks (a), the difference in number of yardsticks (b), and local slope (c), as a function of yardstick size (in pixels) for the seventh construction iteration in a Koch curve (Table III).

Table III. *D* Values for the Early Iterations in the Construction of a Koch Curve

iteration	D^a
1[b]	1.00 ± 0.00
2	1.04 ± 0.01
3	1.13 ± 0.01
4	1.17 ± 0.01
5	1.19 ± 0.01
6	1.22 ± 0.01
7	1.22 ± 0.01
∞	1.26...

[a] Yardstick range: 3.5–114.4 pixels. All correlation coefficients, –0.9990 or better. [b] Length of initiator: 430 pixels. Smallest edge length on the video screen in higher iterations: approximately $^1/_3$, $^1/_9$, etc., of that value.

one-third of the initiator, one-ninth, etc.) one would obtain the "true" fractal dimension, however, nothing in eq 1 restricts the choice of experimental yardsticks. It is also clear that the computed *D* values for regular objects like Figure 8a and, e.g., the third iteration of Koch curve will depend on the range of yardstick chosen and its location relative to the regular-feature size. This warning against

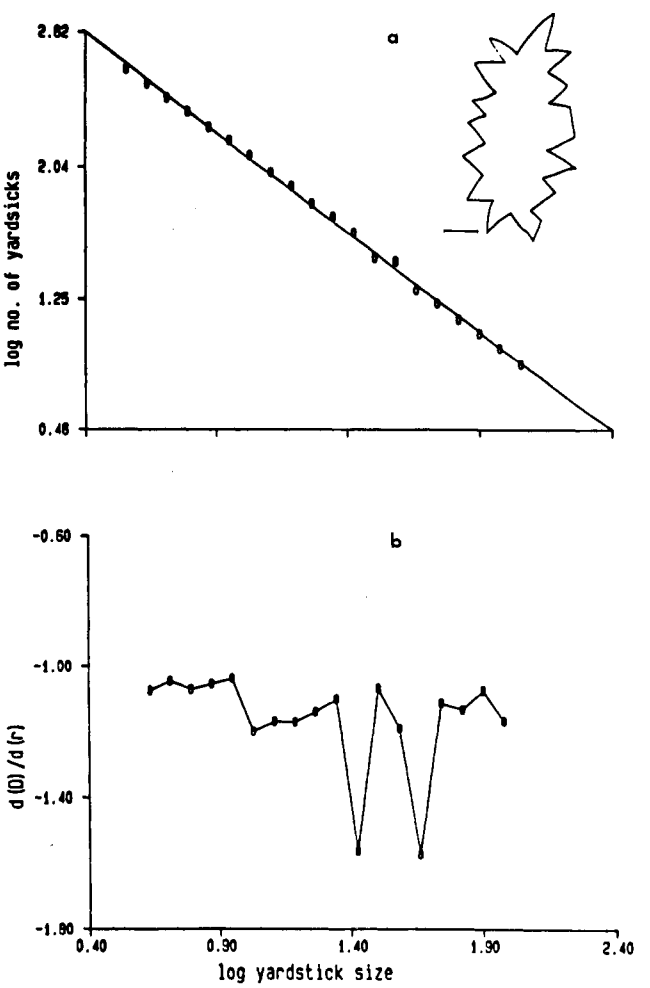

Figure 10. Number of yardsticks (a) and local slope (b), as a function of yardstick size (in pixels), for a reference particle taken from Orford et al.[15]

the automatic use of eq 1 on nonrandom objects is necessary, since a number of authors have done it and obtained questionable results (see, e.g., the quite regular reference particle analyzed in ref 15; Figure 10a in this article).

The fractal dimension and its self-similarity interpretations are basically statistical concepts. For instance, the surface fractal dimension we obtained from adsorption studies[6] were the result of data collected from the equivalent of 10^6 adsorbent particles × 10^5 slices = 10^{11} boundary lines per experiment! The question is, then, what interpretation should be given to *D* values obtained from analyses of single objects which reveal random irregularity, like the examples analyzed in section 3 or even like the object in Figure 11a, which yields $D = 1.13 \pm 0.01$ (correlation coefficient, –0.999).

It seems to us that for all objects analyzed in section 3, the single line analyses provide at least a crude evaluation for the fractal dimension of the whole object or of a collection of similar objects. Thus, the $D = 1.20 \pm 0.01$ obtained for the Pt/C catalyst, from an arbitrarily chosen limited zone, carries information on the low irregularity of the whole object. Interest in single-object irregularity rather than in large assemblies is of course scientifically legitimate. More than that, local variations of irregularity may be a useful "fingerprint" of the object or of the mechanism that formed it, and since the standard analysis employed in section 3 seems to be insufficiently sensitive for detection of the finer features of a line, it seemd to us necessary to develop and use more sensitive tools. Of the

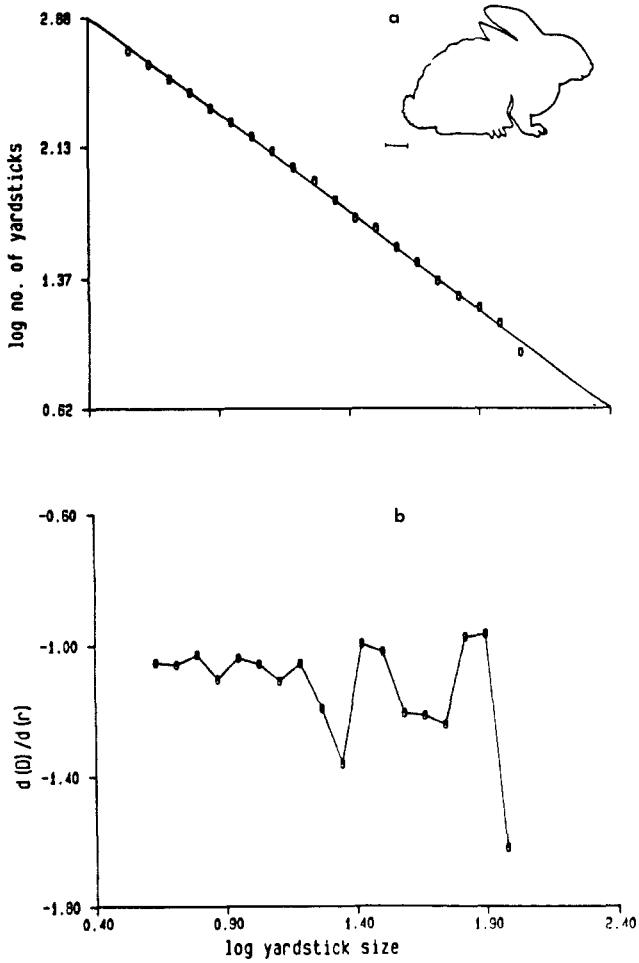

Figure 11. Number of yardsticks (a) and local slope (b), as a function of yardsticks size (in pixels) for an arbitrary object.

sensitive analyses available, the following two proved to reveal significantly more information on the boundary lines.

(a) Analysis of the Increase in Length as a Function of Yardstick Size. For the ith yardstick:

$$n_i = kr_i^{-D}$$

therefore

$$n_i - n_{i+1} = kr_i^{-D}\left[1 - \left(\frac{r_{i+1}}{r_i}\right)^{-D}\right]$$

For a fractal object only, and for a fixed r_{i+1}/r_i, this becomes

$$n_i - n_{i+1} = k'r_i^{-D} \qquad (3)$$

We chose $r_{i+1}/r_i = 1.2$ and tested whether eq 3 is obeyed in our objects. The increased sensitivity of eq 3 compared to eq 1 is immediately evident, e.g., in the sawtooth case (Figure 8b) for which the barely visible information around $r = 10$ in Figure 8a is greatly enhanced. The straight line is indeed much worse. See Figure 2b, Figure 8b, and Table IV.

(b) Determination of Local Slope.[13,14] The local "fractal dimension" was calculated for every yardstick by fitting a straight line for the values of that yardstick and its smaller and larger neighbors, i.e., dD/dr vs. r (see all figures). Whereas the first method is useful in locating *regularities*, the derivative analysis reveals both regularities and *drifts in D*. Sutherland's floc shows a D drift from $D = 1.1$ to 1.5 (Figure 5b), Medalia's floc drifts from $D = 1.0$ to 1.25 (Figure 6b), the catalyst drifts from $D = 1.0$ to 1.2 (Figure 3b), the silica drifts from $D = 1.0$ to 1.8 (Figure 4b), and so on. Thus, it seems that self-similarity in these objects, as might have been inferred from the analyses in section 3, is in fact quite questionable at the single-object level. On the other hand, the effect of small changes in resolution is clearly displayed by the derivative method. The shape of the derivative curve was found to be insensitive to variations in starting points. It remains to be established whether processes, which are local in nature and which occur on or in statistical fractal environments, are governed by the local non-self-similar or even non-fractal properties of the environment or whether they are governed by its statistical properties. Diffusion on fractal surfaces, currently investigated in our laboratory, is an example.

Table IV. Fractal Dimensions of Various Objects

object	figure[a]	fractal dimens from eq 3	corr coeff	fractal dimens from eq 1[c]
protein (α-cobratoxin)[b]	2	1.11 ± 0.03	−0.994	1.13 ± 0.01
Pt black catalyst	3	1.15 ± 0.04	−0.999	1.20 ± 0.01
LiChrospher Si 4000	4	1.20 ± 0.05	−0.983	1.36 ± 0.03
floc size 601 (I)	5	1.20 ± 0.03	−0.993	1.29 ± 0.01
floc size 601 (II)	5	1.23 ± 0.05	−0.989	1.28 ± 0.01
Medalia's floc	6	1.03 ± 0.02	−0.997	1.10 ± 0.01
milled surface (profilometry)		1.27 ± 0.09	−0.961	1.25 ± 0.02
sawtooth	8	1.1 ± 0.1	−0.912	1.09 ± 0.01
Koch curve	9	1.34 ± 0.21	−0.838	1.22 ± 0.02
reference particle	10	1.2 ± 0.1	−0.944	1.18 ± 0.01
arbitrary object (rabbit)	11	1.06 ± 0.05	−0.982	1.13 ± 0.01

[a] Yardstick range: 3.6–114.4 pixels. A 50-pixel reference line is displayed in all figures. [b] All proteins in Table I give virtually the same D values from the two equations. [c] All correlation coefficients, −0.999; LiChrosphere, −0.997.

Special care should be taken in the interpretation of experimental $D < 1.2$ values. The examples analyzed in this study show how easy it is to get "good" low D values for any low irregularity line, even for lines that are neither fractals nor self-similar. The original interpretation of Richardson,[20] i.e., an empirical resolution behavior linking yardstick sizes to length, seems to us the safest one to make in these cases.

Finally, we draw attention to two possible error sources in the assumption that an irregular boundary line fully represents the surface. First, as mentioned above, the objects may not be isotropic. Real objects should, in fact, always reveal some degree of nonisotropy. This is apparent to some degree in mouse immunoglobulin and in the ribosomal protein (Table I). Similarly, Lysozyme cross-section boundary lines vary from $D = 1.08$ to 1.27.[28] Second, if the boundary line is of a silhouette then it might be the sum of overlapping horizons. Such overlapping is expected to lower the D values. In the proteins analyses the effect probably exists but to a rather limited extent: for lysozyme we obtain $D = 1.12 \pm 0.01$ compared to 1.17 ± 0.01 from cross-section analysis.[28]

Three-dimensional analysis for a more accurate look at protein surfaces, as well as the development of stereoscopic resolution analysis tools, is in progress.

5. Conclusion

The use of fractal dimensions to describe natural irregularities is growing very fast. As is often the case in rapidly growing fields, conceptual errors are carried along. We feel that this is, to a certain degree, the case in a number of recently reported line analyses. Yet, it is evi-

dent from these and other reports, as well as from the variety of irregular surfaces analyzed here, that the fractal approach has the potential of offering a solution to irregularity problems. This is certainly true at least at the original level of Richardson's interpretation. However, if one looks for self-similarity, then more sensitive tests, of the kind described in this article or analyses of large assemblies should be employed. The simple message of this paper is *beware of fractal rabbits* (Figure 11).

Acknowledgment. We thank Peter Pfeifer for many stimulating discussions and for critical reading of the first draft of this paper. Financial support of the Israel Academy of Sciences is acknowledged. Supported by the F. Haber Research Center for Molecular Dynamics in Jerusalem.

CO and NO Adsorption on NiO: A Spectroscopic Investigation

E. Escalona Platero, S. Coluccia, and A. Zecchina*

Istituto di Chimica-Fisica, Corso, M. D'Azeglio 48, 10125 Torino, Italy

Received January 7, 1985. In Final Form: February 22, 1985

The IR spectra of CO and NO adsorbed on NiO polycrystalline samples characterized by values of the specific surface area between 100–150 and 1–3 $m^2 g^{-1}$ are reported. The spectra become progressively simpler with the decrease of the surface area and the increase of the perfection of the individual cubic crystallites (as shown by the electron micrographs), and their comparison allows the assignment of the modes associated with CO and NO adsorbed on extended {100} faces and geometrical (edges and steps) and atomic defects. Examination of the IR spectra obtained at different coverages reveals that dipole–dipole and chemical effects (similar to those described for metal surfaces) are responsible for marked frequency shifts of the stretching frequency.

Introduction

NiO, MgO, and NiO–MgO solid solutions have the same crystalline (rock salt) structure, a similar lattice parameter, and the same cubic habit: hence they represent an ideal family of solids for investigations concerning the surface properties of Mg^{2+} and Ni^{2+} (both isolated and clustered) located in well-defined geometrical situations. The interaction of CO and NO with MgO and MgO–NiO solid solutions has been investigated in detail[1-4] by IR spectroscopy and the results can be briefly summarized as follows:

(a) CO. (i) CO does not interact at room temperature with 5-fold coordinated (both isolated and clustered) ions located on {100} facelets of cubic microcrystals; only at 77 K weak Mg^{2+}–CO (σ) and Ni^{2+}–CO ($\sigma-\pi$) adducts are formed which are characterized by stretching frequencies in the 2160–2140-cm^{-1} range. (ii) The room temperature interaction of CO with the ions located on edges and steps (and corners and other defects as well) is much more complex because it involves not only the cations but also the O^{2-} anions.

Apparently on both MgO and NiO–MgO solid solutions, the interaction mechanism shows a common feature: it leads to the simultaneous production of reduced and oxidized species following the parallel schemes

$$2O^{2-} + (n+1)CO \rightarrow {CO_3^{2-}}_{ads} + (CO)_n^{2-} \qquad MgO \qquad (1)$$

$$2O^{2-} + Ni^{2+} + 5CO \rightarrow {CO_3^{2-}}_{ads} + Ni^0(CO)_4 \qquad MgO\text{–}NiO \qquad (2)$$

where the negative species are in close interaction with the Mg^{2+} ions and $Ni(CO)_4$ forms, with a coordinatively unsaturated $Mg^{2+}O^{2-}$ pair, the surface complex

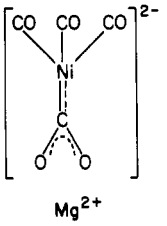

whose structure has been characterized by isotopic exchange experiments[2] and proved by direct $Ni^0(CO)_4$ chemisorption on MgO.[5]

On concentrated solid solutions also reduced polinuclear species have been observed. The relative proportion of mononuclear and polynuclear species depends not only upon the aggregation state of the Ni^{2+} ions but also upon the CO pressure (which favors the formation of the mononuclear species). The redox process previously described is not the only one occurring on low-coordinated sites: in fact, room temperature stable Mg^{2+}–CO (σ) is also formed in a concerted way. At 77 K the reduction of Ni^{2+} ions located on exposed situations does not occur, and surface $Ni^{2+}(CO)_n$ adducts absorbing at 2100–2050 cm^{-1} are observed.

(b) NO. (i) NO does not interact at room temperature with Mg^{2+} ions located on {100} faces of both MgO and MgO–NiO solid solutions. At 77 K, on the contrary, the following process occurs

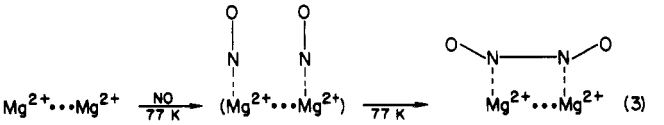

(1) Guglielminotti, E.; Coluccia, S.; Garrone, E.; Cerruti, L.; Zecchina, A. *J. Chem. Soc., Faraday Trans. 1*, **1979**, *75*, 96.
(2) Zecchina, A.; Spoto, G.; Coluccia, S.; Guglielminotti, E. *J. Chem. Soc., Faraday Trans. 1*, **1984**, *80*, 1875.
(3) Zecchina, A.; Spoto, G.; Coluccia, S.; Guglielminotti, E. *J. Chem. Soc., Faraday Trans 1*, **1984**, *80*, 1891.
(4) Escalona Platero, E.; Spoto, G.; Zecchina, A. *J. Chem. Soc., Faraday Trans 1*, in press.
(5) Guglielminotti, E.; Zecchina, A.; Boccuzzi, F.; Borello, E. In "Growth and Properties of Metal Clusters"; Elsevier Scientific: Amsterdam, 1980; p 165.

0743-7463/85/2401-0407$01.50/0